Relation between oxidation kinetics and reactant transport in an aqueous foam

Pierre Trinh, Alesya Mikhailovskaya, Grégory Lefèvre, Nadège Pantoustier, Patrick Perrin, Elise Lorenceau, Benjamin Dollet, Cécile Monteux

Relation between oxidation kinetics and reactant transport in an aqueous foam

Pierre Trinh[1], Alesya Mikhailovskaya[1†], Grégory Lefèvre[2], Nadège Pantoustier[1], Patrick Perrin[1], Elise Lorenceau[3], Benjamin Dollet[3] and Cécile Monteux[1]

1. Soft Matter Science and Engineering, CNRS, ESPCI, PSL University, Sorbonne University, 10 rue Vauquelin, 75005 Paris
2. Chimie ParisTech, PSL Research University, CNRS, Institut de Recherche de Chimie Paris (IRCP), F-75005 Paris, France
3. Univ. Grenoble Alpes, CNRS, LIPhy, 38000 Grenoble, France

Abstract

Hypothesis – Aqueous foams are expected to constitute exquisite particularly suitable reactive medium for the oxidation of metals, since the reactant H^+ can be supplied through the continuous liquid phase, while the reactant O_2 can be transported through the gas bubbles.

Experiments – To test this hypothesis, we investigated the oxidation of a metallic copper cylinder immersed in an aqueous foam. To study the relation between the transport of these reactants and the kinetics of the chemical reaction we use a forced drainage setup which enables us to control both the advection velocity of the H^+ ions through the foam and the foam liquid fraction.

Findings – We find experimentally that the mass of dissolved copper presents a maximum with the drainage flow rate, and thus with the foam liquid fraction. Modeling analytically the transfer of H^+ and O_2 through the foams enables us to show that this non-monotonic behavior results from a competition between the advective flux of H^+ ions and the unsteady diffusion of O_2 through the thin liquid films which tends to be slower as the area of the thin liquid films decreases with Q and the liquid fraction. This study shows for the first time how to optimize the foam structure and drainage flow in reactive foams in which the reactants are present both in the liquid and gaseous phases.

Keywords

Aqueous foams, leaching, oxidation kinetics, diffusion, advection

† Current affiliation : Institut de Chimie et des Matériaux, CNRS, 94320 Thiais, France

INTRODUCTION

Aqueous foams are composed of gas bubbles dispersed in a continuous aqueous phase. They are stabilized by surfactant layers adsorbed at the liquid/air interfaces. Foams are used in a wide range of applications such as water treatment (1) or decontamination (2-4), where their low liquid volume fraction is advantageous as it enables to reduce the volumes of liquid to be cleaned or recycled. In these processes and in flotation (5-12), species such as ions (5,6), minerals (7-9) or radioactive elements (2-4) adsorb and concentrate at the surface of bubbles, and can then be collected easily as they float atop the aqueous solution. Foams can also be used as chemical reactors for reactions where one of the reactants is a gas, for example for hydrogenation using H_2 or oxidation by O_2 (13-15). In such applications the large interfacial area enables a high contact area between the reactants in the gaseous and liquid phases. Recently we used foams in another field of chemistry, hydrometallurgy, which consists in oxidizing metals into metal ions in order to dissolve them in aqueous phase (16). Hydrometallurgy was traditionally used for the mining industry for ore extraction and is also a promising route for the recovery of metals from waste of electrical and electronic equipment (WEEE), such as Platinum Group Metals, gold, silver or copper (17-22). To decrease the environmental footprint of this recovery process and reduce the amounts of leaching effluents usually generated, we recently showed in a proof-of-concept article that foams can be used to oxidize and dissolve metals (16). We studied the oxidation of a copper plate into copper ions Cu^{2+} when put in rotation in a foam obtained with air bubbles. In our system the oxidant was the O_2 contained in the bubbles and the H^+ ions were present in the continuous liquid phase according to the following reaction

$$2Cu + O_2 + 4H^+ \rightleftharpoons 2Cu^{2+} + 2H_2O. \quad (1)$$

Using foams, we achieved a much higher dissolution rate than for aqueous solutions because the reactive gas O_2 transfers very quickly through the foam. It follows that controlling the atmosphere above the foams is crucial, since a fast transfer of O_2 takes place in the foam from the atmosphere towards the copper surface.

In the present article, our goal is to quantify how the transfer of O_2 and H^+ controls the kinetics of the chemical reaction in a situation where metallic copper as a cylinder shape is immobile in the foam. We perform forced drainage experiments which consist in applying a drainage flow of the surfactant/H^+ solution through the foams at a controlled flow rate Q. This set up enables us to control the advection of the H^+ ions through the foams and to impose a homogeneous and variable liquid fraction ϕ in the foam. We measure the mass of dissolved copper as a function of the drainage flow rate Q and liquid fraction ϕ. We show that the dissolved mass presents a maximum with Q and ϕ,which results from a competition between (i) the diffusion/advection flux of H^+ ions in the continuous phase, which increases with Q, and (ii) the diffusion flux of O_2 from the atmosphere toward the copper cylinder,

which slows down with ϕ as it induces a decrease of the surface area of the thin liquid films through which O_2 passes from one bubble to another. Our results emphasize that both the foam structure and the drainage velocity play a key role in the transfer of the gaseous and liquid reactants hence on the reaction kinetics.

MATERIALS AND METHODS

Reactants

Foams are generated from hydrochloric acid solutions (0.1 or 0.5 mol/L) containing the non-ionic surfactant BrijO10 ($C_{18}H_{35}(OCH_2CH_2)_nOH$, n~10) at the concentration of 0.05 mol/L. The gas used is filtered ambient air, with traces of C_6F_{14}, to slow down the coarsening of the foam bubbles (23), which is incorporated by bubbling air into a bottle filled with liquid C_6F_{14}.

Foam preparation

A column of foam is produced by injecting gas through a porous glass disk (porosity: 16-40 or 40-100 µm), inserted at the bottom of a Plexiglass column (3 x 3 x 30 cm). The copper cylinder (diameter: 2 cm, height: 3 cm) is immersed before each experiment into a 0.1 M nitric acid solution for ten minutes to remove eventual possible copper oxide layer, and is then immersed in the foam at a distance $H_m = 16\ cm$ from the top of the foam.

The air with the traces C_6F_{14} is injected with the flow rate of 20 ml/min to the column containing 50 ml of the foaming solution. The column is completely filled within about 10 minutes with the foam of average bubble diameter 67 µm for the porous disk of porosity 16-40 µm, and 205 μm for the porous disk of porosity 40-100 µm. The produced foam is immediately subjected to the drainage and to the coarsening, the latter, however, is significantly decelerated by the presence of C_6F_{14} in the gas phase. The coarsening rate is similar to the one observed for other aqueous foams prepared with the same gas composition (24). We have not observed any coalescence of the bubbles during the whole experiment, which suggests that the consumption of O_2 has no noticeable effect on foam stability.

The foam is left to drain freely for two hours before the start of the forced drainage.

Forced drainage experiment

The experimental setup is presented on Figure 1. The foaming solution is injected above the foam at a controlled flow rate Q with a syringe pump (Harvard Apparatus PHD Ultra) operated with four syringes (volume 140 mL per syringe, Sherwood Pastic Monoject). This moment is taken as the initial time $t = 0$ for experiments. Forced drainage experiments are then performed for three hours. The height H_l of the drained solution is maintained nearly constant (± 3 mm) using a first reservoir (container 1) linked through a valve to a column output. The first container then flows into a second container (container 2) where the solution is recovered.

The bubble sizes, polydispersity and foam liquid fraction are both obtained during the experiment with a telecentric lens and gluing a prism with a 45° angle on the column surface (25). At this foam age, the mean bubble diameter $\langle D_B \rangle$ is 180 μm for the porous disk of porosity 16-40 µm, or 400 μm for the porous disk of porosity 40-100 µm, and the foam polydispersity σ ranges from 20% to 45%.

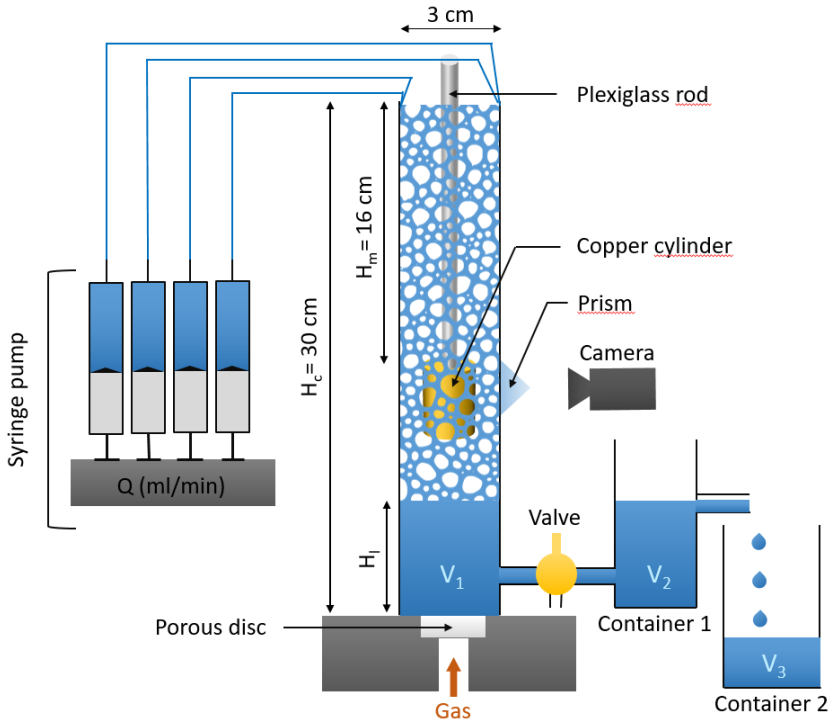

Figure 1: Forced drainage experimental setup.

The mass of dissolved copper is determined by taking foaming solution samples that are then analyzed with an Inductively Coupled Plasma - Optical Emission Spectrometry (ICP-OES). Every 30 minutes, samplings are performed in 3 distinct locations: at the valve (between the column output and the first container), in the first container, and in the second container. ICP-OES analysis of these samples gives the local copper ions concentration respectively in the drained solution at the bottom of the column, and in each of the two containers. The copper dissolved amount versus time is then determined with Eq. (2):

$$n(Cu)_{dis} = [Cu^{2+}]_1^{ICP} V_1 + [Cu^{2+}]_2^{ICP} V_2 + [Cu^{2+}]_3^{ICP} V_3 \qquad (2)$$

where $n(Cu)_{dis}$ is the amount of substance of the dissolved copper, $[Cu^{2+}]_i^{ICP}$ is the molar concentration of copper ions in the location i and V_i is the volume of the corresponding probe. An example of image of the foams is given in Figure 2a where one can see that the areas corresponding to thin films are in light shade, while those corresponding to the Plateau borders are in dark shade. We use Image J to measure the mean bubble equatorial radius $\langle R_B^{eq} \rangle$. The surface liquid fraction ϕ_s is obtained by taking the ratio of the white area to the total surface, and the volume liquid fraction ϕ is obtained using

$$1 - \phi_s = \left(1 - \sqrt{\frac{\phi}{\phi_c}}\right)^2 \qquad (3)$$

where ϕ_c is the critical liquid fraction equal to $\phi_c \approx 0.36$, for disordered polydisperse foams and $\phi_c \approx 0.26$ for ordered monodisperse foams (25-27).

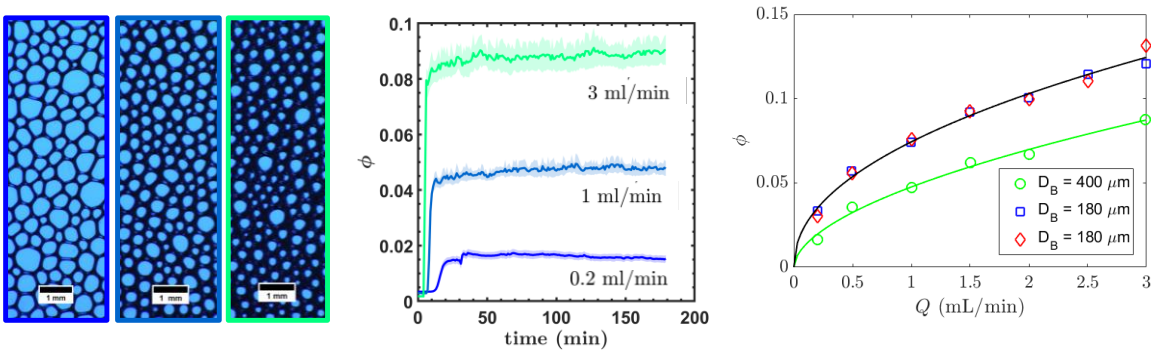

Figure 2 .a) Snapshots of the foams during a forced drainage experiment at three different flow rates Q, 0.2, 1 and 3 ml/min corresponding to three different liquid fractions. b)-Time evolution of the liquid fraction over time for three different flow rates, c) Liquid fraction evolution with Q for two different bubble sizes. The two curves are the best fits by power laws: $\phi = 0.0732Q^{0.512}$ for $D_B = 180$ µm, and $\phi = 0.0468Q^{0.599}$ for $D_B = 400$ µm, where Q is expressed in mL/min.

The time evolution of the liquid fraction ϕ for three flow rates shown in Fig. 2b, reveals that after a transient regime of at most 30 minutes, the liquid fraction remains constant over time. In Fig. 2c, the evolution of the plateau value for the liquid fraction ϕ is plotted as a function of the flow rate Q for two bubble sizes and two HCl concentrations 0.1 and 0.5 M. It can be seen that the liquid fraction, which typically ranges between 0.02 and 0.15, increases with the flow rate Q and is lower for the largest bubble size for a given flow rate. As expected, varying the acid concentration at fixed bubble size (180 µm) does not affect the relation between ϕ and Q.

This surprising dependence of the liquid fraction of a foam in forced drainage with bubble size is not predicted by theoretical models. Although we have no explanation for this fact, a similar trend has also been observed by Carrier et al. (28).

RESULTS & DISCUSSION

Mass of dissolved copper and observation of the cylinders

We measure the total mass of dissolved copper m_{Cu} as a function of the flowrate Q for two HCl concentrations and two bubble sizes (Fig. 3). Remarkably, the three curves present a maximum with

Q. At low Q, the mass of copper increases with the flow rate and with the HCl concentration. Above a critical flow rate, the dissolved mass decreases with Q and the effect of the HCl concentration for a given bubble size becomes negligible at the highest flow rates. Moreover, for the largest bubbles, a lower mass of copper is dissolved. These results suggest that at low Q, the chemical reaction may be limited by the flux of H^+: increasing Q leads to an increase in the amount of H^+ ions reaching the surface of the copper plate hence to an increase of the mass of copper dissolved. At higher flow rates, we suggest that the chemical reaction may be limited by the transfer of O_2 diffusing from one bubble to another through the thin liquid films. Indeed, as Q increases, the area of the thin liquid films decreases which can possibly hinder the transfer of O_2. In the next Sections we model the reactant transfers to test these hypotheses.

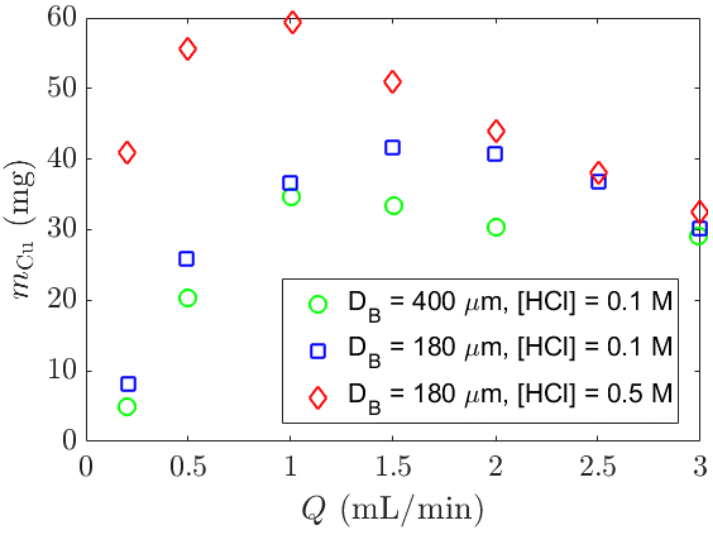

Figure 3. Mass of dissolved copper as a function of the flow rate. Blue squares : [HCl]= 0.1M, D_B = 180 µm ; red diamonds [HCl] =0.5 M, D_B=180 µm; green circles : [HCl]=0.1 M, D_B=400 µm.

Modeling of H^+ and O_2 transfers in foams and link with reaction kinetics

Advective transfer of H^+ through foams

To estimate the H^+ ions flux that can reach the copper surface, we use a standard advection/diffusion approach (29). The H^+ ions flow downwards through the foam at a velocity u controlled by the forced drainage, and diffuse since the H^+ ions are consumed by the chemical reaction occurring at the copper surface, and a concentration gradient is established between this surface and the bulk of the foam (Fig. 4). A depletion zone then grows with a characteristic thickness δ_{H^+}. Without advective flux, this depletion zone would expand according to the scaling law $\delta_{H^+} = \sqrt{D_{H^+} t}$,

with D_{H^+} the diffusion coefficient of H^+ ions and t the time. The forced drainage advection flow opposes the growth of this depletion zone, since it replenishes the foam with fresh H^+ ions. This results in a steady depletion zone of length δ_{H^+}, where ions at a distance $d < \delta_{H^+}$ from the cylinder reach the copper surface by diffusion and take part in the dissolution reaction. This length δ_{H^+} can thus be determined as shown below.

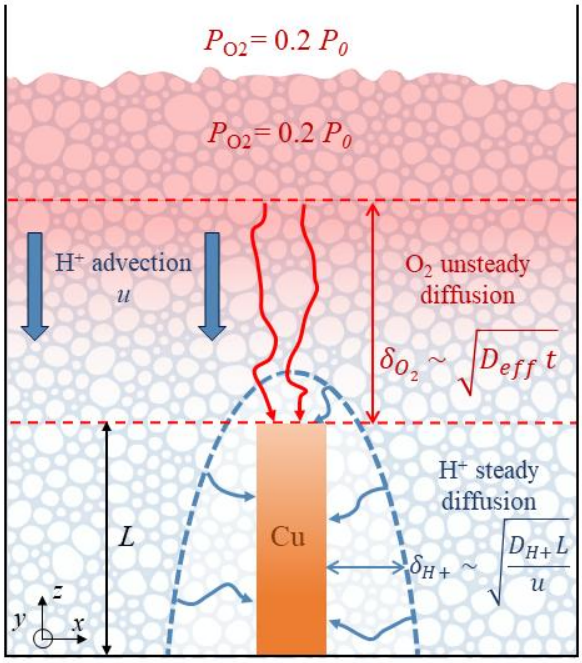

Figure 4 Sketch of the main types of transport for H^+ and O_2 considered in this study.

The diffusive flux of H^+ ions (in mol/s) is:

$$J_{H^+} = \frac{D_{H^+}\Delta C}{\delta_{H^+}} S_{yz}^{l}, \qquad (4)$$

with $S_{yz}^{l} \simeq 2\pi(\mathrm{R_{cyl}})\mathrm{L}\phi$ the surface covered by the liquid (whence the factor ϕ) at the distance δ_{H^+} from the copper surface, and ΔC the H^+ concentration difference between the copper surface and far from the copper surface. Assuming that the H^+ concentration far from the copper surface is equal to the injected foaming solution concentration $C_{H^+}^{0}$, and that the ions concentration on copper surface is negligible with respect to $C_{H^+}^{0}$, we have

$$J_{H^+} = 2\frac{D_{H^+}C_{H^+}^{0}}{\delta_{H^+}} \pi(R_{cyl})L\phi, \qquad (5)$$

with R_{cyl} the copper cylinder radius, and L its length.

Then assuming that δ_{H+}writes as a diffusive boundary layer $\delta_{H+}\sim\sqrt{D_{H+}t}$ and that $t\sim L/u$, it comes:

$$\delta_{H^+} = \sqrt{\frac{D_{H^+}L}{u}}. \tag{6}$$

In the forced drainage stationary regime, the mean velocity flow *u* is:

$$u = \frac{Q}{\phi(S_{col} - \pi R_{cyl}^2)}, \tag{7}$$

with S_{col} the column cross-section.

By taking $D_{H^+} = 9.31 \times 10^{-9}\, m^2/s$ (30,31), δ_{H^+} ranges from 1.2 mm to 513 µm for the explored flow rates, a value in agreement with the hypothesis $\delta_{H^+} \ll R_{cyl}$. Using equations 5, 6 and 7, H^+ ions flux J_{H^+} reaching the copper surface is obtained:

$$J_{H^+} = A_{H^+}C_{H^+}^0\sqrt{Q\phi} \;\; with \;\; A_{H^+} = cste = 2\,\pi\,R_{cyl}\sqrt{\frac{D_{H^+}L}{S_{col}-\pi R_{cyl}^2}}. \tag{8}$$

If O_2 were always present in excess at the copper surface, the theoretical dissolved copper mass m_{Cu}^{H+} would then equal:

$$m_{\mathrm{Cu}}^{H+} = B_{H^+}C_{H^+}^0\sqrt{Q\phi} \;\; with \;\; B_{H^+} = cste = 2\,\pi\,R_{cyl}\sqrt{\frac{D_{H^+}L}{S_{col} - \pi R_{cyl}^2}}\,\nu_{H^+/Cu}\,\Delta t\,M(Cu), \tag{9}$$

with $\nu_{H^+/Cu} = 2$, the ratio between stoichiometric number of H^+ ions and Cu^{2+}, $\Delta t = 180\,mins$ the experiment duration, and $M(Cu) = 63.546\,g/mol$ the copper molar mass.

The experimental dissolved masses m_{Cu} versus the theoretical dissolved mass $m_{\mathrm{Cu}}^{H+}$are shown in Figure 5. The black line corresponds to the model. At low *Q*, we obtain a very good agreement between the experimental data and the model without any fitting parameter. However, at higher *Q*, a large discrepancy between the model and the data is observed, since the model where H^+ is always the limiting reactant predicts a continuous increase in dissolved copper mass, while our data show a decreasing dissolved mass. This suggests that the diffusive transfer of O_2 may limit the reaction for high *Q* and has to be taken into account.

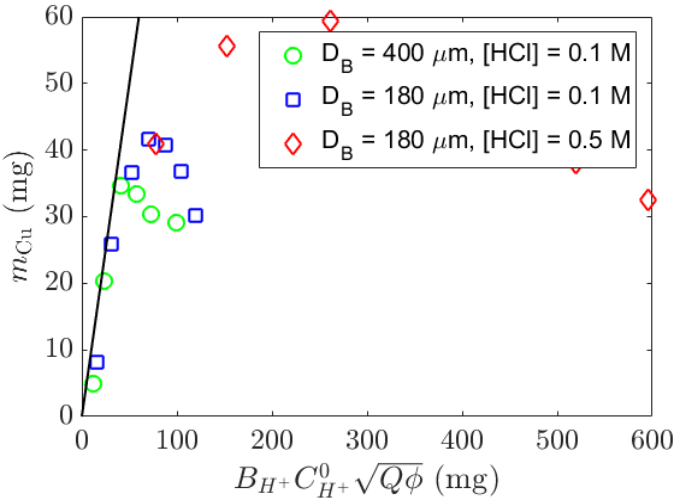

Figure 5. Comparison of the experimental results of mass of dissolved copper (blue, green and red data points) with the theoretical model given by Eq. (9) (black line).

Modeling the transfer of O_2 through the foam

As oxygen is consumed at the copper surface, it is progressively depleted in the vicinity of the copper cylinder and a concentration gradient of O_2 develops close to its surface. Oxygen can be supplied by two transport mechanisms: (i) a diffusion mechanism of gaseous oxygen through the foam, (ii) a convection mechanism whereby oxygen is brought by forced drainage similarly to the H^+ ions. Unlike for the case of H^+, the advective flux of O_2 brought by the forced drainage flow is negligible against the diffusion mechanism in our experimental conditions (see the paragraph focused on this conclusion in SI). Therefore, the flux of oxygen results from an unsteady diffusion process of the gaseous oxygen with a depletion zone progressing through the foam first in the direction perpendicular to the copper cylinder axis and then extending above the cylinder toward the top of the foam column (Fig. 4).

To determine how the depletion zone grows over time and how the oxygen diffuses toward the cylinder, we need to estimate the diffusion coefficient of this process. We assume that the oxygen concentration in each bubble is instantaneously equilibrated, and that the limiting transport process is the oxygen diffusive transfer through the thin liquid films between adjacent bubbles of different oxygen concentration. In analogy to the case of coarsening foams, first described by Mason and Princen (32,33), we define the permeability of the thin liquid films to gas transfer, k_{film} which has the dimensions of a velocity in m/s. We note that in coarsening foams made of air, the diffusion of gas through the thin liquid films is driven by gradients of gas activity due to variations of Laplace pressure, while in our case the driving force for the O_2 transfer is a gradient of concentration in the gas bubbles. According to Princen, Overbeek and Mason (32), the transport of gases through soluble monolayers is governed by simple Fickean diffusion through aqueous pores between the surfactant molecules. Hence, neglecting the resistance due to the surfactant adsorbed layers. the film permeability writes $k_{film} = \alpha D_{O_2}/h$, with $\alpha = 0.032$ is the Henry's constant, $D_{O_2} = 2 \times 10^{-9}$ m²/s,

the diffusion coefficient of oxygen in water, and h the thickness of the whole film. For the surfactant solution used in this study, Mikhailovskaya et al. (34) measured film thicknesses of individual self-standing thin liquid films of $h = 15$ nm, constant for capillary pressures up to 10 kPa, which is much larger than the Laplace pressures calculated for bubbles diameters between 180 and 400 µm (less than 2 kPa). For such film thicknesses we deduce a film permeability $k_{film} = 4$ mm/s. Moreover, we assume that, in the spirit of the *border-blocking* model (35) the transfer through Plateau borders is negligible. Using the same approach as Mason and Princen for coarsening foams, we define an effective diffusivity for the oxygen transfer through the foams as (32,33,36):

$$D_{eff} = \kappa k_{film} D_B f(\phi), \quad (10)$$

with κ a dimensionless constant of order one, and where f is the fraction of a bubble surface covered by thin films (the other part of the surface being occupied by Plateau borders and nodes). Hilgenfeldt et al. derived the evolution of the film area with the liquid fraction for a monodisperse foam $f(\phi) = \left(1 - 1.52\sqrt{\phi}\right)^2$ (35), which is a quickly decreasing function of ϕ (f is halved when ϕ increases from 0 to 0.037). As a consequence, the effective diffusivity is a decreasing function of ϕ, as confirmed by the measurements of Saulnier et al. (36). However, as we shall discuss later, in our case the surface fraction can be evaluated experimentally and exhibits a similar dependency with ϕ, but with an empirical value of the exponent of 2.4 slightly larger than the theoretical value of 2 (see Fig. SI1 and its caption).

Assuming a value of κ of the order of one for the two bubble diameters studied D_B=180 and 400 µm and since in the range of liquid fraction considered here, $f(\phi)$ typically varies between 0.6 and 0.15, we obtain $D_{eff} \sim k_{film} D_B \approx 10^{-6}$ m²/s. This effective gas diffusion coefficient through the foam is three orders of magnitude larger than the diffusion coefficient of O_2 in the liquid phase, suggesting a very rapid transport of the gas through the media.

We now focus of the influence of the geometry of the experiment on the diffusion flux of O_2. At the early stages of the chemical reaction, oxygen can be supplied all around the copper cylinder. However, the lateral boundaries become important after a time of order $t_{lat} = (a_{col} - R_{cyl})^2 / 4D_{eff}$, where $(a_{col} - R_{cyl})/2$ is the characteristic distance between the copper cylinder and the lateral boundaries. The order of magnitude of this time is $t_{lat} = \frac{(0.03-0.01)^2}{4\times10^{-6}} = 10^2$ s, which is much lower than the duration of our experiments. At times larger than t_{lat}, the oxygen initially present at the lateral sides of the cylinder is exhausted, and the flux comes mostly from the top part of the copper cylinder. Since the experiments run typically over 10^4 s, we assume that we are always in this situation. Therefore, the order of magnitude of the oxygen flux is:

$$J_{O_2} = \pi R_{cyl}^2 C_{O_2} \frac{D_{eff}}{\delta_{O_2}} \quad (11)$$

with $C_{O_2} = x_{O_2}/v_m = 9$ mol/m^3 the molar concentration of oxygen in the atmosphere (with $x_{O_2} = 0.21$ the molar fraction of oxygen in the atmosphere, and $v_m = 0.024$ m^3/mol the molar volume of gas

in the lab conditions), and $\delta_{O_2} \approx \sqrt{D_{eff}t}$ the typical distance over which the concentration gradient of oxygen develops in the foam at a given time *t*. Hence,

$$J_{O_2} = \pi R_{cyl}^2 C_{O_2} \sqrt{\frac{D_{eff}}{t}} \quad (12)$$

which is a decreasing function of time with a short-time divergence. Of course, if the lateral boundaries were much farther apart so that t_{lat} would be larger than the duration of the experiments, the flux would be isotropic and this would lead to different scalings of Eqs. (11) and (12); in particular, the factor πR_{cyl}^2 should then be replaced by the total surface area of the cylinder.

Since the flux of H^+ is constant over time, while that of oxygen is decreasing with limits $\lim_{t\to 0} J_{O_2} = +\infty$ and $\lim_{t\to+\infty} J_{O_2} = 0$, there exists a crossover time t^* below which H^+ is the limiting reactant, and above which oxygen is the limiting reactant. Taking into account the stoichiometry of the reaction, the crossover time is reached when $J_{H^+} = 4J_{O_2}$. Solving this equation using Eqs. (8) and (12) yields the following expression:

$$t^* = \frac{D_{eff}}{Q\phi}\left(\frac{4\pi R_{cyl}^2 C_{O_2}}{A_{H^+} C_{H^+}^0}\right)^2 = \frac{4}{Q\phi}\frac{R_{cyl}^2(S_{col} - \pi R_{cyl}^2)}{L}\frac{D_{eff}}{D_{H^+}}\left(\frac{C_{O_2}}{C_{H^+}^0}\right)^2 \quad (13)$$

Let us estimate this crossover time. In all experiments, the following geometrical factor has a fixed value: $\frac{R_{cyl}^2(S_{col}-\pi R_{cyl}^2)}{L} = 2.0$ cm^3, and we always have (see previous sections) $D_{H^+} = 9.31 \times 10^{-9}$ m²/s and $C_{O_2} = 9$ mol/m^3. The other parameters may vary, depending on the bubble size (via the diffusion coefficient), the liquid fraction (because $t^* \propto f(\phi)/\phi$), the flow rate or the concentration of H^+. We take as representative values: $D_{eff} \approx 10^{-6}$ m²/s, $\phi = 0.1$, $Q = 1\ mL/min = 1.7 \times 10^{-8}$ m^3/s and $C_{H^+}^0 = 0.1$ mol/L, which gives:$t^* = 4 \times 10^3\ s$.

This typical time is almost two orders of magnitude larger than t_{lat}, which validates our simplified geometrical description of the unsteady diffusion of oxygen. It is two to three times lower than the total duration of the experiments: hence, estimating both fluxes is important, although varying the parameters, some experiments are limited by H^+ all along (low flow rate, acid concentration and liquid fraction or large bubbles) and some mostly by oxygen (large flow rate, acid concentration and liquid fraction, small bubbles).

Most importantly, this analysis yields the following estimate of the rate of dissolution:

$$\dot{m}_{Cu}^{O2} = M_{Cu} \times \begin{cases} \frac{1}{2}J_{H^+} & t < t^* \\ 2J_{O_2} & t > t^* \end{cases}, \quad (14)$$

hence after integration:

$$m_{Cu}^{O2} = M_{Cu} \times \begin{cases} \frac{1}{2}J_{H^+}t & t < t^* \\ \frac{1}{2}J_{H^+}t^* + 4\pi R_{cyl}^2 C_{O_2}\sqrt{D_{eff}}\left(\sqrt{t} - \sqrt{t^*}\right) & t > t^* \end{cases} \quad (15)$$

To validate this theoretical modeling, we compare equations (14) and (15) with experimental data of dissolved copper mass for all studied regimes. Since the ϕ(Q) experimental curves shown in Figure 2c show different dependence for the two investigated bubble diameters, we use two different phenomenological functions and inject them into the expression of D_{eff}. This allows us to calculate the mass of dissolved copper for all the experimental situations investigated experimentally with only one fitting parameter, κ, defined above in Eq. (10). For the three experimental data sets, the proposed model fits well the experimental curves giving m_{Cu} as a function of Q as shown in Figure 6a. Two points deserve to be discussed. First, the existence of an optimum Q for which m_{Cu} is well reproduced. The larger the bubble size the lower the optimum flow rate. Then, we compare the value of κ obtained for the different curves. For the two curves corresponding to D_B=180 µm, the values of κ are logically very close and equal to 2.13 and 2.27. However, for D_B = 400 µm, we obtain a value of 0.49, significantly smaller, although remaining in the order of 1.

To go further, we use these values of κ to plot the evolution of D_{eff} with Q in Figure 6b. As expected, D_{eff} does not depend on the HCl concentration and decreases with Q, since the film area also decreases with Q. The two curves for D_B = 180 µm logically nearly overlap since the values of κ and the functions used to describe evolution of the foam liquid fraction with flow rate are identical. However, we observe that these two curves are shifted from the one obtained for D_B = 400 µm. Indeed, when the size of the bubbles varies, both functions used to describe foam wetting, as well as the values of κ, are modified.

The effect of the bubble size on κ could come from subtle physico-chemical effects. Specifically, to obtain a stable foam for several hours, traces of C_6F_{14} are added to the ambient air. This gas being almost totally insoluble in water, it does not diffuse between the bubbles and counteracts by osmotic effect the Ostwald ripening. Thus, even two bubbles with different radii can remain thermodynamically stable. Yet, it has also been recently shown that by adsorbing onto the hydrophobic layers of the film surfactants, C_6F_{14} creates an additional barrier to gas transport via the film, thereby reducing the effective permeability (38). In our case, since foams made of small bubbles exhibit a larger surface-to-volume ratio than those made of large bubbles, it is likely that the thickness of the C_6F_{14} adsorbed film is higher for the large bubbles than for the small bubbles, thus reducing more significantly the permeability of foams made of large bubbles. This subtle mechanism would indeed lead to a lower value of κ for large bubbles than for small bubbles. This calls for further dedicated studies on the precise role of C_6F_{14} on gas transfer in foams with gas mixtures, with a detailed tracking of the time evolution of the size and gas contents of individual gas bubbles, which is beyond the scope of the present study.

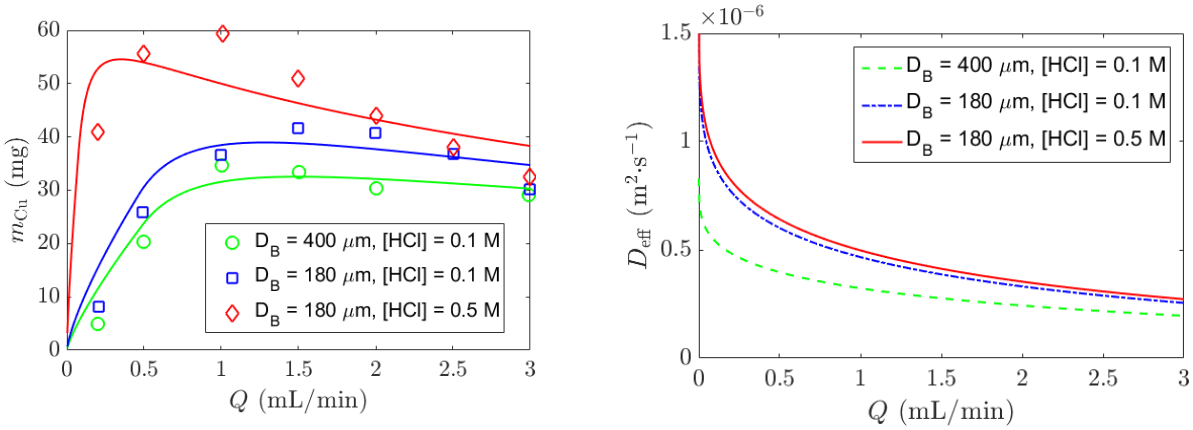

Figure 6. a) Comparison of the mass of dissolved copper measured experimentally and predicted Equation (15). b) values of D_{eff} obtained from Eq. (10) using values of κ that enable to fit Eq. (15) with the experimental data.

To conclude this discussion, although the detailed transfer of O_2 and H^+ at the scale of the Plateau borders and films is not described by our model, which considers the foams as an effective medium, we can obtain an insight into the transfer in the lubricating film between the foam and the copper cylinder by analyzing the lateral surface of the copper cylinder using SEM microscopy after three hours of experiment (Figure 7). Hexagonal patterns can be observed on the copper cylinder which correspond to areas where the copper has been preferentially dissolved. As shown in Figure 7d, these patterns correspond to the areas where the lubricating films between the bubbles and the copper cylinder are the thinnest hence the transfer of O_2 toward the cylinder is the fastest. In qualitative agreement with the border-blocking model (35), the transfer of O_2 through the thicker liquid menisci between the lubricating films is probably more difficult, and results in a lower dissolution.

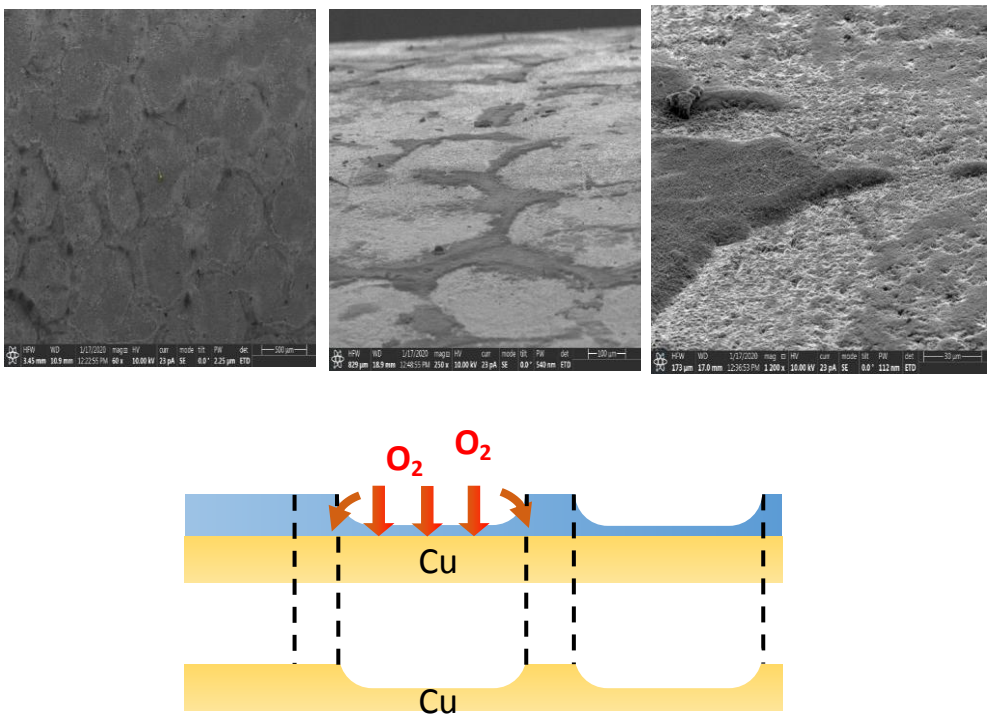

Figure 7 Surface of the copper cylinder after an experiment. A, B, C,: SEM images of the copper cylinder surface after forced drainage experiment ([HCl] =0.1M, D_B = 400 µm, Q=0.2 ml/min); D. Schematic drawing showing the transfer of O_2 through the films and menisci of the wetting film between the foam and the cylinder

CONCLUSION

Key findings – We investigate the relation between the kinetics of copper oxidation reaction and the transport of gaseous and liquid reactants in aqueous foams in order to find optimal conditions for the leaching process. Using a forced drainage set up we control both the advection velocity of the H^+ ions through the foams as well as the foam liquid fraction which increases with the flow rate Q. We suggest that at low Q, the chemical reaction may be limited by the flux of H^+ and at high Q by the transfer of O_2, whose diffusion is hindered due to the decrease of the liquid film area. We find experimentally that the mass of dissolved copper presents a maximum with the drainage flow rate and hence with the foam liquid fraction. Modeling analytically the H^+ and O_2 transfers through the foams, we show that this non-monotonic behavior is due to a competition between the advective flux of H^+ ions which increases with Q and the non-stationary diffusion of O_2 through the thin liquid films which tends to be slower for larger Q as the area of the thin liquid films decreases with the liquid fraction.

Hypothesis, new concepts and innovations – This study shows for the first time how to optimize the foam structure and drainage flow in reactive foams in which the reactants are present both in the liquid and gaseous phases. Futhermore foams under forced drainage are ideally suited as reaction media for reactions involving a gas and a solute, because they combine a fast supply of gas (through the bubbles), and an efficient supply of the solute (through the Plateau borders) while using low amounts

of liquid. Hence, it is foreseeable that they could be used as very efficient media in processes as important as e.g. carbon dioxide capture.

Key improvements compared to the literature – Despite great potential of foams as media for chemical reactions, the research in this domain is quite scarce. Most of the studies are dedicated to the investigation of the interplay between the foam stability and the rate of the chemical conversion within the foam liquid phase (42-49), but the number of works considering the reaction involving both the liquid and the gas foam phases is very limited (13-16). Furthermore none of these published articles neither controlled nor modeled precisely the transfers of reactants. The originality of the present study lies in the fact that we use a controlled rate of forced drainage which enables to unravel the influence of drainage velocity and liquid fraction on the reactant transfers both in the liquid and gaseous phases. Moreover we provide for the first time a quantitative model of these reactant transfers which will help future studies to find optimum conditions to optimize the reaction yield.

Our vision for future work – Further enhancement in understanding of the reactants' transport in foams can be made if the variation of the liquid film thicknesses with the flow rate are measured directly in the foam. In the present work we assume that foam film thickness is the same as for individual self-standing films since the drainage dynamics was previously shown to be in excellent agreement in both cases (34). At the same time, an evolution of the foam film thickness can be observed during the forced drainage experiment (28). Despite the key importance of quantitative characterization of this evolution, it remains unknown as it is difficult to assess. Accurate measurements of the film thickness evolution *in situ* within the foam require an experimental technique that is both non-destructive and insensitive to foam opacity. Small-angle neutron scattering (SANS) meets these requirements and it has been successfully applied to the study of the evolution of structural parameters of foams (39), in particular, of the film thickness during their ageing (40,41). Using of SANS in a forced drainage experiment will allow to reveal the dependence of the thin film thickness on the foam liquid fraction in a controlled way.

ACKNOWLEDGEMENTS

We acknowledge financial support from Agence Nationale de la Recherche (grant number ANR-17-CE08-0016 FOAMEX), ADEME and Fondation Del Duca. We acknowledge A. L. Biance, M. C. Jullien and D. Mottin for stimulating discussions concerning the reactant transfer through the foams and O. Diat, D. Bourgeois, S. Guignot for discussions about copper leaching.

BIBLIOGRAPHY

1. J. Rubio, M. L. Souza, R. W. Smith, Overview of flotation as a wastewater treatment technique, *Miner. Eng.* **15**, 139155 (2002).

2. L. Stoica, D. Filip, G. Filip, A. Razvan, R. Radulescu, Removal of ^{226}Ra(II) from uranium mining and processing effluents, *J. Radioanal. Nucl. Chem.* **229**, 139-142 (1998).

3. C. Dame, C. Fritz, O. Pitois, S. Faure, Relations between physicochemical properties and instability of decontamination foams, *Colloids Surf. A* **263**, 210–218 (2005).

4. R. Deleurence, T. Saison, F. Lequeux, C. Monteux, Time scales for drainage and imbibitions in gelified foams: application to decontamination processes, *Soft Matter* **11**, 7032-7037 (2015).

5. F. M. Doyle, Ion flotation - its potential for hydrometallurgical operations. *Int. J. Miner. Process.* **72**, 387-399 (2003).

6. C. Micheau, D. Dedovets, P. Bauduin, O. Diat, L. Girard, Nanoparticle foam flotation for caesium decontamination using a pH-sensitive surfactant. *Environ. Sci.* **6**, 1576-1584 (2019).

7. R. Houot, Beneficiation of iron-ore by flotation - review of industrial and potential applications. *Int. J. Miner. Process.* **10**, 183-204 (1983).

8. X. Ma, W. J. Bruckard, R. Holmes, Effect of collector, pH and ionic strength on the cationic flotation of kaolinite. *Int. J. Miner. Process.* **93**, 54-58 (2009).

9. A. M. Gaudin, and D. W. Fuerstenau. Quartz flotation with anionic collectors. *Trans. Am. Inst. Min.* **202**, 66-72 (1955).

10. B. Burghoff, Foam fractionation applications. *J. Biotech.* **161**, 126-137 (2012).

11. W. D. Lambert, L. Du, Y. Ma, V. Loha, V. Burapatana, A. Prokop, R. D. Tanner, N. B. Pamment, The effect of pH on the foam fractionation of beta-glucosidase and cellulase. *Bioresour. Tech.* **87**, 247-253 (2003).

12. J. Lambert, R. Mosko, I. Cantat, P. Cloetens, J. A. Glazier, F. Graner, R. Delannay, Experimental growth law for bubbles in a moderately “wet” 3D liquid foam. *Phys. Rev. Lett.* **104**, 248304 (2010).

13. A. Feng, D. Debovets, Y. Gu, S. Zhang, J. Sha, X. Han, M. Pera-Titus, Organic foams stabilized by biphenyl-bridged organosilica particles. *J. Colloid Interface Sci.* **617**, 171–181 (2022).

14. S. Zhang, D. Dedovets, A. Feng, K. Wang, M. Pera-Titus, Pickering interfacial catalysis for aerobic alcohol oxidation in oil foams, *J. Am. Chem. Soc.* **144**, 1729–1738 (2022).

15. D. Dedovets, S. Zhang, J. Leng, M. Pera-Titus, Microfluidic device for monitoring catalytic events on armored bubbles, *Adv. Mater. Interfaces* **9**, 220759 (2022).

16. P. Trinh, A. Mikhailovskaya, M. Zhang, P. Perrin, N. Pantoustier, G. Lefèvre, C. Monteux, Leaching foams for copper and silver dissolution: A proof of concept of a more environmentally friendly process for the recovery of critical metals. *ACS Sustainable Chem. Eng.* **9**, 14022–14028 (2021).

17. T. Hino, R. Agawa, Y. Moriya, M. Nishida, Y. Tsugita, T. Araki, Techniques to separate metal from waste printed circuit boards from discarded personal computers. *J. Mater. Cycles Waste Manag.* **11**, 42-54 (2009).

18. Y. H. Zhou, K. Q. Qiu, A new technology for recycling materials from waste printed circuit boards. *J. Hazard. Mater.* **175**, 823-828 (2010).

19. P. Quinet, J. Proost, A. van Lierde, Recovery of precious metals from electronic scrap by hydrometallurgical processing routes. *Miner. Metall. Process.* **22**, 17-22 (2005).

20. F. P. C. Silvas, M. M. Jiménez Correa, M. P. K. Caldas, V. T. de Moraes, D. C. R. Espinosa, J. A. S. Tenório, Printed circuit board recycling: Physical processing and copper extraction by selective leaching, *Waste Manag.* **46**, 503-510 (2015).

21. O. Tsydenova, M. Bengtsson, Chemical hazards associated with treatment of waste electrical and electronic equipment. *Waste Manag.* **31**, 45-58 (2011).

22. S. Ilyas, J. Lee, R. Chi, Bioleaching of metals from electronic scrap and its potential for commercial exploitation, *Hydrometallurgy* **131**, 138-143 (2013).

23. D. Weaire, V. Pageron, Frustrated froth: evolution of foam inhibited by an insoluble gaseous component, *Philos. Mag. Lett.* **62**, 417-421 (1990).

24. A. Mikhailovskaya, V. Trappe, A. Salonen, Colloidal gelation, a means to study elastocapillarity effects in foam, *Soft Matter*, **16**, 2249-2255 (2020).

25. E. Forel, E. Rio, M. Schneider, S. Beguin, D. Weaire, S. Hutzler, W. Drenckhan, The surface tells it all: relationship between volume and surface fraction of liquid dispersions. *Soft Matter* **12**, 8025–8029 (2016).

26. R. Höhler, Y. Yip Cheung Sang, E. Lorenceau, S. Cohen-Addad, Osmotic pressure and structures of monodisperse ordered foam. *Langmuir* **24**, 418-425 (2008).

27. A. Maestro, W. Drenckhan, E. Rio, R. Höhler, Liquid dispersions under gravity: volume fraction profile and osmotic pressure. *Soft Matter* **9**, 2531-2540 (2013).

28. V. Carrier, S. Destouesse, A. Colin, Foam drainage: A film contribution? *Phys. Rev. E* **65**, 061404 (2002).

29. T. M. Squires, R. J. Messinger, S. R. Manalis, Making it stick: Convection, reaction and diffusion in surface-based biosensors. *Nat. Biotechnol.* **26**, 417–426 (2008).

30. G. Baysinger, L. I. Berger, R. N. Goldberg, H. V. Kehiaian, K. Kuchitsu, G. Rosenblatt, D. L. Roth, D. Zwillinger, *Handbook of Chemistry and Physics*, 85th ed.; CRC Press LLC (2000).

31. S. H. Lee, J. C. Rasaiah, Proton transfer and the mobilities of the H+ and OH- ions from studies of a dissociating model for water, *J. Chem. Phys.* **135**, 124505 (2011).

32. H. M. Princen, J. T. G. Overbeek, S. G. Mason, The permeability of soap films to gases: II. A simple mechanism of monolayer permeability, *J. Colloid Interface Sci.***24**, 125-130 (1967).

33. H. M. Princen, S. G. Mason, The permeability of soap films to gases, *J. Colloid Sci.* **20**, 353-375 (1965).

34. A. Mikhailovskaya, E. Chatzigiannakis, D. Renggli, J. Vermant, C. Monteux, From individual liquid films to macroscopic foam dynamics: A comparison between polymers and a nonionic surfactant. *Langmuir* **38**, 10768–10780 (2022).

35. C. D. Schimming, D. J. Durian, Border crossing model for the diffusive coarsening of two-dimensional and quasi-two-dimensional wet foams, *Phys. Rev. E* **96**, 032805 (2017).

36. S. Hilgenfeldt, S. A. Koehler, H. A. Stone, Dynamics of coarsening foams: Accelerated and self-limiting drainage, *Phys. Rev. Lett.* **86**, 4704-4707 (2001).

37. L. Saulnier, W. Drenckhan, P. E. Larré, C. Anglade, D. Langevin, E. Janiaud, E. Rio, In situ measurement of the permeability of foam films using quasi-two-dimensional foams, *Colloids Surf. A.* **473**, 32-39 (2015).

38. C. Hadji, B. Dollet, H. Bodiguel, W. Drenckhan, B. Coasne and E. Lorenceau, Impact of fluorocarbon gaseous environments on the permeability of foam films to air, *Langmuir* **36**, 13236-13243 (2020).

39. A. Mikhailovskaya, L. Zhang, F. Cousin, F. Boué, P. Yazhgur, F. Muller, C. Gay, A. Salonen, Probing foams with neutrons, *Adv. Colloid Interface Sci.* **247**, 444-453 (2017).

40. M. A. V. Axelos, F. Boué, Foams as viewed by small-angle neutron scattering, *Langmuir* **19**, 6598-6604 (2003).

41. J. Lamolinairie, B. Dollet, J. L. Bridot, P. Bauduin, O. Diat, L. Chiappisi, Probing foams from the nanometer to the millimeter by coupling small-angle neutron scattering, imaging, and electrical conductivity measurements, *Soft Matter* **18**, 8733-8747 (2022).

42. S.E. Friberg, J.-H. Fang, Foams from aqueous systems of polymerizable surfactants, *J. Colloid Interface Sci*., **118,** 543-552 (1987).

43. K.-Y. Lee, L.L.C. Wong, J.J. Blaker, J.M. Hodgkinson, A. Bismarck, Bio-based macroporous polymer nanocomposites made by mechanical frothing of acrylated epoxidised soybean oil, *Green Chem*., **13**, 3117-3123 (2011).

44. S. Andrieux, A. Quell, C. Stubenrauch, W. Drenckhan, Liquid foam templating – A route to tailor-made polymer foams, *Adv. Colloid Interface Sci.* **256**, 276-290 (2018).

45. B. Feneuil, P. Aimedieu, M. Scheel, J. Perrin, N. Roussel, and O. Pitois, Stability criterion for fresh cement foams, *Cem. Concr Res.* **125**, 105865 (2019).

46. R. Zowada and R. Foudazi, Polyfoam: Foam-Templated Microcellular Polymers, *Langmuir*, **36**, 7868-7878 (2020).

47. M. L. Dabrowski and C. Stubenrauch, Methacrylate-based polymer foams with controllable pore Sizes and controllable polydispersities *via* foamed emulsion templating, *Adv. Eng. Mater*., **23**, 2001013 (2021).

48. H. Yu, Y. Zhu, A. Hui, F. Yag, A. Wang, Removal of antibiotics from aqueous solution by using porous adsorbent templated from eco-friendly Pickering aqueous foams, *J. Environ. Sci.*, **102**, 352-362 (2021).

49. J. Trosseille, G. Panczer, C. Martinet, M. Le Merrer, *Phys. Rev. Applied* **18**, 034078 (2022).

50. R. Sander, Compilation of Henry law's constant (version 4.0) for water as solvent, *Atmos. Chem. Phys.* **15**, 4399-4981 (2015).

Supporting information

1. Surface area of the thin liquid films in contact with the copper cylinder

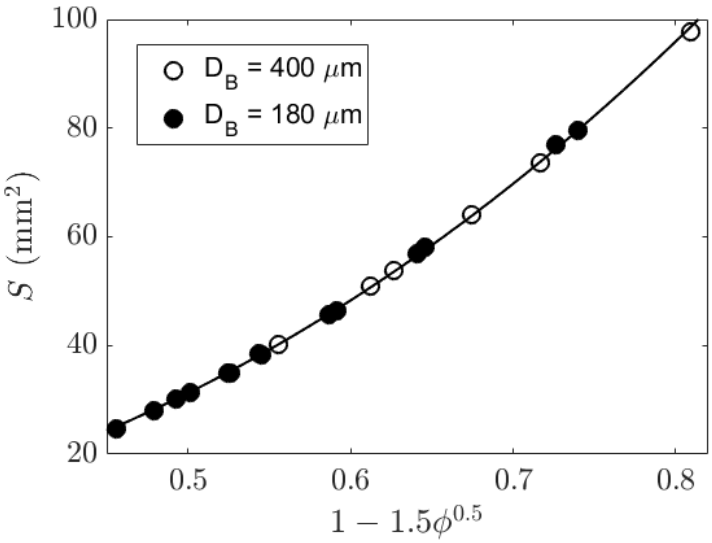

SI1. *Evolution of the total surface area of the thin films, S, in contact with the upper surface of the copper cylinder as a function of Q taking S = ϕ_s * πR_{cyl}^2. The curve is a fit by the law* $S = c_1(1 - 1.5\phi^{0.5})^{c_2}$ *with* c_1 *and* c_2 *free fitting parameters. In particular, the best fit is achieved for* $c_2 = 2.41$. *Since the surface fraction covered by films equals* $f(\phi) = S(\phi)/S(\phi = 0)$, *this implies* $f(\phi) = (1 - 1.5\phi^{0.5})^{2.41}$.

2. Comparison of oxygen transport by diffusion vs. by advection

In the manuscript, we model the transport of oxygen by diffusion through the foam. However, the forced drainage also supplies, by advection, oxygen dissolved in the Plateau borders, and we must

discuss the relative importance of these two modes of transport, diffusive and advective. To do so, we consider two concentration fields for oxygen: the field of gaseous oxygen in the bubbles, denoted *c*, and the field of dissolved oxygen in the liquid Plateau borders, denoted *C*, and we establish the equations which they obey.

First, we assume that the two concentration fields are related through Henry's law, valid at the gas/liquid interface (whence the subscripts int):

$$C_{int} = \alpha c_{int},$$

with α Henry's constant for O_2. If both concentrations are expressed as molar concentrations, we have (49) $\alpha = 0.032$. Henry's condition imposes a gaseous concentration at the contact with the Plateau borders which may differ from that in the `bulk' of the bubble: the corresponding difference generates an exchange flux which we now quantify. To proceed, we make two simplifying assumptions concerning the Plateau borders: (i) instead of accounting for their exact circular triangular cross-section, we assume that they have a circular cross-section of radius R_{PB}; (ii) we consider the dry foam limit for which $R_{PB} \ll D_B$. Then, in the vicinity of a given Plateau border, the concentration field obeys a local diffusion equation, which we assume to be quasi-steady. From the two aforementioned hypotheses, this diffusion equation has the following solution:

$$c = c_B + (c_{int} - c_B)\frac{R_{PB}}{r},$$

where c_{int} is the concentration at the interface with the Plateau border, located at $r = R_{PB}$ with *r* the distance from the center of the Plateau border, and c_B is the concentration in the `bulk' of the bubble. Hence, using Fick's law, there is a diffusive flux per unit length of the Plateau borders which equals:

$$j = -2\pi R_{PB} D_{O_2} \left.\frac{\partial c}{\partial r}\right|_{r=R_{PB}} = 2\pi D_{O_2}(c_{int} - c_B).$$

In what follows, in view of hypothesis (ii), we identify c_B to the `mesoscopic' concentration field *c* at the scale of the foam, which evolves according to the effective diffusivity discussed in the manuscript; here, the flux *j* acts as a source term for this field, and we can write:

$$\frac{\partial c}{\partial t} = D_{eff}\nabla^2 c + \beta_{PB} j,$$

with β_{PB} the mean cumulated length of Plateau borders per unit volume of the foam. A simple scaling law yields $\beta_{PB} = \tilde{\beta}_{PB}/D_B^2$, with $\tilde{\beta}_{PB}$ a dimensionless constant of order unity. Combining all results, we get the following equation:

$$\frac{\partial c}{\partial t} = D_{eff}\nabla^2 c + \frac{2\pi D_{O_2}\tilde{\beta}_{PB}}{D_B^2}\left(\frac{C}{\alpha} - c\right), \quad (16)$$

where the source term couples the two concentration fields.

To get an equation for *C*, we express the conservation of oxygen in a portion of Plateau border of length dz, where the liquid flows at velocity u_{PB} assumed constant. The flux of oxygen crossing a section of Plateau border at given *z* equals $\pi R_{PB}^2 u_{PB} C(z)$, hence the conservation of oxygen imposes that $\pi R_{PB}^2 u_{PB} C(z) - \pi R_{PB}^2 u_{PB} C(z + dz) = j\, dz$, or:

$$\pi R_{PB}^2 u_{PB} \frac{\partial C}{\partial z} = -j = -2\pi D_{O_2}\left(\frac{C}{\alpha} - c\right). \quad (17)$$

Hence, the system of equations (16) and (17) describe the evolution of the concentration of oxygen both in the gas phase and in the liquid phase of the foam, over both actions of diffusion and convection.

To discuss the relative importance of diffusion and convection, it is useful to make these equations dimensionless. The relevant scale for the oxygen concentration in the gas phase is the concentration of oxygen in the atmosphere $C_{O_2} = 9$ mol/m^3, and from Henry's law, the relevant scale for the oxygen concentration in the liquid phase is αC_{O_2}. Hence, we define the following dimensionless concentration fields:

$$\tilde{c} = \frac{c}{C_{O_2}}, \quad \tilde{C} = \frac{C}{\alpha C_{O_2}}.$$

Since we are interested in the distribution of oxygen at the scale of the copper cylinder where the reaction occurs, we can make *z* dimensionless by a length built from the cylinder radius R_{cyl} or height *L*. Both these lengths are centimetric, hence the choice of the scaling length is not critical; we take R_{cyl} to be consistent with the discussion of the unsteady diffusion in the manuscript, which suggests R_{cyl}^2/D_{eff} as the relevant time scale. Hence, we define the dimensionless time and space coordinate:

$$\tilde{z} = \frac{z}{R_{cyl}}, \quad \tilde{t} = \frac{D_{eff}t}{R_{cyl}^2}.$$

Making equations (16) and (17) dimensionless and combining them yields:

$$\frac{\partial \tilde{c}}{\partial \tilde{t}} = \tilde{\nabla}^2 \tilde{c} + Pe \frac{\partial \tilde{C}}{\partial \tilde{z}}, \quad \tilde{C} - \tilde{c} = \frac{R_{PB}^2 u_{PB} \alpha}{2 R_{cyl} D_{O_2}} \frac{\partial \tilde{C}}{\partial \tilde{z}}.$$

The first equation has the form of a convection-diffusion equation, with a Péclet number defined as:

$$Pe = \frac{\pi R_{cyl} R_{PB}^2 u_{PB} \alpha}{D_{eff} D_B^2},$$

which compares the importance of convection and diffusion. To get an estimate of this Péclet number, we take the orders of magnitude: $\phi \approx R_{PB}^2 / D_B^2$ and $u_{PB} \approx Q / S_{col} \phi$, hence:

$$Pe \approx \frac{\pi R_{cyl} \alpha}{D_{eff}} \frac{Q}{S_{col}} \approx 6 \times 10^{-2},$$

taking the largest flow rate of the experiments: $Q = 3$ mL/min, and $D_{eff} \approx 10^{-6}$ m²/s. Hence, this parameter is small, which justifies that advection remains a negligible mode of transport of oxygen in our range of experimental parameters.